ATLAS NOTE

ATLAS-CONF-2011-103

July 21, 2011

Search for the Standard Model Higgs boson produced in association with a vector boson and decaying to a b-quark pair with the ATLAS detector at the LHC

The ATLAS Collaboration

Abstract

This note summarizes results of the first ATLAS direct search for the Standard Model Higgs boson in the mass range $110 < m_H < 130$ GeV when produced in association with a W or Z boson and decaying to $b\bar{b}$. No evidence for Higgs boson production is observed in a dataset of 7 TeV pp collisions corresponding to 1.04 fb^{-1} of integrated luminosity, recorded by the ATLAS experiment at the LHC in 2011. Upper limits on Higgs boson production cross-sections for the channels considered are presented and discussed.

1 Introduction

The search for the Standard Model [1–3] Higgs boson [4–9] is one of the most important goals of the Large Hadron Collider (LHC) [10–12] physics program. If the Higgs boson mass, m_H, is less than twice the W boson mass, m_W, the Higgs boson will decay into two b-quarks with a high branching fraction [13]. In this low mass region the production process $gg \to H$ dominates, but the background to $H \to b\bar{b}$ from Standard Model processes is expected to be prohibitively large. However, the production process of the Higgs boson in association with an electroweak boson VH (where V=Z or W), whilst having a cross-section less than half the size of the $gg \to H$ cross-section, is likely to be a more promising process to identify $H \to b\bar{b}$ decays due to the reduction in background and the improved trigger signature provided by the leptonic decays of the vector boson. The production cross-section for WH is approximately twice as large as that for ZH. These channels are important contributors to Higgs boson exclusion limits at low Higgs boson mass obtained at the Tevatron [14–17]. At the LHC the background from top-quark production is expected to be significantly larger. Studies of the sensitivity of ATLAS to VH-production at low Higgs boson mass were done on Monte Carlo simulations of high integrated luminosity and focused on highly boosted events, where both the Higgs boson and the vector boson have very large p_{T} and the two b-jets from the Higgs boson decay merge together into a single large jet with high p_{T} [18]. The study presented here, performed on a small fraction of the expected LHC integrated luminosity considered in the above mentioned sensitivity study, employs a simple and robust cut-based analysis to search for the Higgs boson in the VH channels, and provides a first useful determination of the backgrounds for future searches.

An important irreducible background for both WH and ZH arises from vector boson production in association with 2 b-quark jets ($Vb\bar{b}$). This background will be considerably smaller in the WH channel because $\sigma(Wb\bar{b})/\sigma(Wjj)$ is approximately a factor of four smaller than $\sigma(Zb\bar{b})/\sigma(Zjj)$. However, the WH channel will have a much more significant background from top-quark pair production due to the presence of two W bosons and two b-jets from the decay of the top quarks in the final state.

This note presents searches in the $ZH \to \ell\ell b\bar{b}$ and $WH \to \ell\nu b\bar{b}$ channels, where ℓ is either an e or μ. The final state for the $ZH \to \ell\ell b\bar{b}$ channel is the same as that used in Higgs boson searches at high m_H, where $m_H > 2m_Z$, using the process $H \to ZZ \to \ell\ell b\bar{b}$ [19]. Most of the event selection, Monte Carlo samples and background estimations used in the high mass search apply also to the analysis presented here. The $ZH \to \ell\ell b\bar{b}$ channel is characterized by two high transverse momentum leptons of the same flavour originating from the decay of a Z boson and two high momentum b-jets. The main backgrounds in this channel are from Z+jets, diboson, top-quark and QCD multijet production. The $WH \to \ell\nu b\bar{b}$ channel is characterized by a single high transverse momentum lepton (e or μ) and missing transverse energy consistent with originating from the electroweak decay of a W boson, and two high momentum b-jets. The main backgrounds in this channel are from top-quark, W+jets, diboson and QCD multijet production.

The ATLAS detector has been described elsewhere [20]. This note presents the dataset used, the definitions employed for electrons, muons, jets, b-tagged jets and missing transverse momentum, the selection criteria for the two analyses, the estimation of backgrounds, the systematic uncertainties, and then the results. In addition, results relevant for an ongoing search for a high transverse momentum (boosted) Higgs boson decaying to $b\bar{b}$ are presented in Section 9.

2 Data and Monte Carlo Samples

This section describes the data sample used in this analysis along with the relevant signal and background processes and the Monte Carlo generators used to model them. All Monte Carlo samples are generated for a centre-of-mass energy of 7 TeV and passed through the full ATLAS detector simulation [21] which

is based on the GEANT 4 [22] program.

2.1 Data Sample

The data used in this analysis were recorded by the ATLAS experiment during the 2011 LHC run at a centre-of-mass energy of $\sqrt{s}$ = 7 TeV and represent an integrated luminosity of 1.04 fb^{-1} [23]. The data are required to satisfy a number of conditions ensuring essential elements of the ATLAS detector were operational with good efficiency while the data were collected.

2.2 Signal Samples

The signal $WH \to \ell\nu b\bar{b}$ and $ZH \to \ell\ell b\bar{b}$ events where $\ell = e, \mu, \tau$ are modelled using Monte Carlo (MC) events produced by the PYTHIA 6.421 [24] event generator. The PYTHIA generator is interfaced to PHOTOS [25] for final-state radiation and TAUOLA [26] for the simulation of τ decays. The τ leptons are simulated to account for the small fraction of additional signal events that arise from the decay of the τ via $\tau \to \nu_\tau l \nu_l$ where l is either an electron or muon. Five samples are generated in the Higgs boson mass range between 110 GeV and 130 GeV. The total cross-sections for Higgs boson production in association with an electroweak vector boson in pp collisions at $\sqrt{s}$ = 7 TeV, as well as their corresponding uncertainties, are taken from Ref. [13]. The central values of the cross-sections, calculated at next-to-next-to-leading-order (NNLO) in QCD corrections [27] and next-to-leading-order (NLO) in electroweak corrections [28], and assuming factorization between the production of a virtual V^* boson and its decay to VH, are shown in Table 1, along with the $H \to b\bar{b}$ decay branching ratio [13, 29], for the Higgs boson mass range of 110 GeV to 130 GeV considered in this note. The decay branching ratios of $W^\pm$ and Z bosons from the Particle Data Group [30] are used assuming lepton universality. The uncertainties on the signal cross-sections are discussed in Section 7.

m_H (GeV)	$\sigma(WH)$ (pb)	$\sigma(ZH)$ (pb)	Branching Ratio $H \to b\bar{b}$
110	0.875	0.472	0.745
115	0.755	0.360	0.705
120	0.656	0.316	0.649
125	0.573	0.278	0.578
130	0.501	0.245	0.494

Table 1: Standard Model Higgs boson production cross-sections at NNLO QCD + NLO EW in pp collisions at $\sqrt{s}$ = 7 TeV for the associated production of a W/Z boson and a Higgs boson, along with the $H \to b\bar{b}$ decay branching ratio, from Ref. [13], for a range of Higgs boson masses.

2.3 Background Samples

The background processes are modelled with several different event generators. The ALPGEN generator [31] interfaced with the HERWIG program [32] for parton showers and hadronization is used to simulate W/Z+jets events. The MC@NLO generator [33], interfaced to HERWIG and JIMMY [34] for the simulation of underlying events, is used for the production of top-quarks and the diboson (ZZ,WZ and WW) MC events. For the WW diboson samples, an additional contribution from gluon-initiated diagrams is modelled using `gg2WW` [35]. The HERWIG generator is used to simulate additional diboson WW samples.

The Standard Model ZZ process is an irreducible background for ZH as the two have the same final state. Its production cross-section has been calculated up to NLO in QCD corrections [36]. The

Process	Generator	$\sigma \times BR$
WH	PYTHIA	See Tab. 1
ZH	PYTHIA	See Tab. 1
$W \to \ell\nu$	ALPGEN	10.46 nb [38, 39]
$Z/\gamma* \to \ell\ell$	ALPGEN, PYTHIA	
$m_{\ell\ell} > 40$ GeV		1.07nb [38, 40]
$m_{\ell\ell} > 60$ GeV		0.989 nb [38, 40]
WW	MC@NLO+gg2WW	46.23 pb [35, 36]
$WW \to l\nu qq$	HERWIG	46.23 pb [35, 36]
WZ	MC@NLO	
$66 < m_{\ell\ell} < 116$ GeV		18.0 pb [36]
ZZ	MC@NLO, PYTHIA	
$66 < m_{\ell\ell} < 116$ GeV		5.96 pb [36]
Top-quark		
$t\bar{t}$	MC@NLO	164.6 pb [41]
$t-$channel	MC@NLO	58.7 pb [36]
$s-$channel	MC@NLO	3.94 pb [36]
$Wt-$channel	MC@NLO	13.1 pb [36]
$b\bar{b} \to \mu\mu$	PYTHIA	73.9 nb
$c\bar{c} \to \mu\mu$	PYTHIA	28.4 nb

Table 2: Monte Carlo programs used for modelling signal and background processes and the cross-sections times branching ratio (BR) used to normalize the different processes. Branching ratios correspond to the decays shown. Where two generators are given the second is used to estimate systematic uncertainties.

MC@NLO generator includes NLO corrections but only models the contribution from on-shell Z bosons. Consequently an alternative sample was produced using PYTHIA. Although only leading-order, this includes the off-shell Z boson and photon contributions which are absent from the MC@NLO generator. This sample is used for cross-checks and to evaluate the systematic uncertainties. Additionally, the ZZ cross-section is scaled up by a factor of ~6% to account for missing gluon pair quark-box diagrams ($gg \to ZZ$) [37].

The background due to QCD multijet production is evaluated from data for the electron channel for both $ZH \to \ell\ell b\bar{b}$ and $WH \to \ell\nu b\bar{b}$ (see Sections 5.4 and 6.4). In the muon channel for the $ZH \to \ell\ell b\bar{b}$ analysis this background is expected to be very small with the only significant contributions from semileptonic $c-$ and b-hadron decays. Samples of $b\bar{b}$ and $c\bar{c}$ production are generated with the PYTHIA 6.421 [24] event generator requiring one of the $b-$ or c-hadrons to decay to a muon with $p_{\mathrm{T}} > 15$ GeV and $|\eta| < 2.5$. In the muon channel for $WH \to \ell\nu b\bar{b}$ the multijet background is estimated from the data.

Table 2 summarizes the programs used for generating MC events and the inclusive cross-sections for normalization of the various background processes. The uncertainties on these cross-sections will be discussed in Section 7.

3 Object Identification and Selection

The identification and reconstruction of electrons, muons, jets and missing transverse energy are briefly described here; further details can be found in Ref. [20].

The leptonic decays of W and Z bosons give rise to isolated high transverse momenta electrons or muons. The lepton identification cuts are tighter in the W channel since there is a higher background from jets misidentified as leptons compared with the Z channel. The kinematic range of the lepton selection is

also more restricted in the W channel than in the Z channel in order to reduce the multijet background and ensure a high reconstruction and trigger efficiency for the case of a single lepton (rather than di-lepton) in the final state.

Electron candidates are reconstructed from electromagnetic calorimeter clusters matched to tracks reconstructed in the inner detector. The clusters must have shower profiles consistent with those expected from an electromagnetic shower. Details of electron reconstruction and identification are described in Refs. [42, 43]. The electron candidates for the Z (W) channels are required to pass the standard ATLAS "medium" ("tight") selection criteria, to have transverse energy $p_{\mathrm{T}} > 20(25)$ GeV and lie within the pseudorapidity coverage of the ATLAS tracking detectors ($|\eta| < 2.47$).

Muon candidates are reconstructed by matching tracks found in the inner detector with either tracks or track segments in the muon spectrometer [44]. Muon candidates in the Z (W) channel are required to have $p_{\mathrm{T}} > 20(25)$ GeV and $|\eta| < 2.5(2.4)$. To avoid double counting, electron candidates that lie within $\Delta R = \sqrt{(\Delta\eta)^2 + (\Delta\phi)^2} < 0.2$ of a selected muon are rejected.

In order to suppress leptons produced in jets, such as those originating from semileptonic decays of b-hadrons, the sum of track transverse momenta in an η-ϕ cone of radius 0.2 around the identified lepton track must be less than $0.1 \times p_{\mathrm{T}}$, where p_{T} is the transverse momentum of the lepton. To further reduce semileptonic decays in the W channel the transverse (longitudinal) distance from the lepton track to the vertex must be less than 0.1 (10) mm and muons are required to have an η-ϕ distance greater than 0.4 to any reconstructed jet satisfying the selection criteria described below.

Jets are reconstructed from topological clusters [45] in the calorimeter using an anti-k_t algorithm [46] with a radius parameter $R = 0.4$. They are calibrated from the electromagnetic energy scale to the hadronic energy scale using a simple p_{T} and η dependent correction factor based on MC simulation and validated on data. Only jets with $p_{\mathrm{T}} > 25$ GeV are considered in the following analysis. In addition, a minimum value of 0.75 is placed on the absolute "jet vertex fraction" (JVF), the fraction of the p_{T} sum of tracks in a jet which are associated to the main primary collision with respect to the p_{T} sum of all the jet tracks. This requirement significantly reduces the effect of pile-up from additional proton-proton interactions [47]. To ensure a good tracking acceptance for the JVF cut, the jets are required to be in the range $|\eta| < 2.5$. Furthermore, a jet is required to have no electron satisfying the selection criteria described above within a distance $\Delta R < 0.4$ around the jet axis.

The missing transverse energy, $E_{\mathrm{T}}^{\mathrm{miss}}$, is measured from the vector sum over all topological clusters in the calorimeters with $|\eta| < 4.5$ together with terms accounting explicitly for selected muons in the event [48]. The calorimeter deposits associated with the muon are subtracted to avoid double counting.

ATLAS b-tagging algorithms are used to distinguish jets containing decays of b-hadrons from those containing only light quarks. These algorithms take advantage of the fact that hadrons containing a b-quark have a significant lifetime ($c\tau \approx 450\ \mu$m). Jets containing such hadrons are primarily identified by reconstructing a secondary decay vertex from the tracks within the jet, or by combining the distance of closest approach to the primary vertex (impact parameter) of all tracks in the jet. Tracks are taken to be associated to a jet if they lie within $\Delta R < 0.4$ of the jet axis.

In this note a combination of the three-dimensional impact parameter information and the output of the secondary vertex finding algorithm is used. The b-tagging cut is chosen so that its efficiency is 70% for $b-$jets in simulated $t\bar{t}$ events while providing a light jet rejection factor of around 50 in simulated $t\bar{t}$ events. The $b-$tagging efficiencies were studied in data with a sample of jets containing muons and with $t\bar{t}$ events, and mis-tagging fractions were studied with a sample of inclusive jets, following the procedures described in Ref. [49]. Scaling factors were derived to account for the small differences observed between the Monte Carlo simulation and the data.

A number of additional corrections and reweighting procedures are applied to Monte Carlo events to account for differences between data and simulation. Events are reweighted to modify the distribution of the number of extra pp interactions due to pile-up to that observed in the data. Corrections for trigger and

lepton identification efficiencies are measured using a tag-and-probe method [50] on selected $Z \to ee(\mu\mu)$ events. The lepton momentum resolution in the detector simulation is found to be slightly better than in data and so a smearing of the measured momenta is applied separately for electrons and muons to match the resolution in the data [51].

4 Event Selection

4.1 Common Event Selection

The $ZH \to \ell\ell b\bar{b}$ and $WH \to \ell\nu b\bar{b}$ analyses both use single lepton triggers with a p_{T} threshold of 18 GeV for muons and 20 GeV for electrons. Both triggers have reached their efficiency plateau for the minimum lepton p_{T} required in the WH search, 25 GeV. For the muon trigger this plateau is around 90% efficient with respect to the offline reconstruction, whereas it is close to 100% efficient for the electron trigger relative to the offline selection. To ensure almost 100% efficiency for the $Z \to ee$ channel, where a cut $p_{\mathrm{T}} > 20$ GeV is required, the single electron trigger is complemented with a $p_{\mathrm{T}} > 12$ GeV di-electron trigger. At very high transverse momentum, $p_{\mathrm{T}} > 100$ GeV, the simulation of the single muon trigger was found to have a lower efficiency than in the data. To compensate for the drop in efficiency, an additional loose single muon trigger, identified in the muon spectrometer only with a p_{T} threshold of 40 GeV, is added to the muon selection.

All triggered events are required to have a reconstructed primary vertex containing at least three tracks. In order to ensure that $E_{\mathrm{T}}^{\mathrm{miss}}$ is well calculated and to remove jets originating from non-physics backgrounds such as those arising from hardware problems, cosmic-ray showers and beam backgrounds, a jet cleaning cut is applied: Any event with a jet of $p_{\mathrm{T}} > 20$ GeV failing the "loose" jet cleaning criteria [52] is rejected.

The $ZH \to \ell\ell b\bar{b}$ and $WH \to \ell\nu b\bar{b}$ channels mainly differ in their selection of the associated Z and W bosons, described in the next sections. The reconstruction of the $H \to b\bar{b}$ decays and the search for a signal above the background expectation in the invariant mass of the di-b-jet system is identical for the two channels.

4.2 Selection of $ZH \to \ell\ell b\bar{b}$ Candidates

After the object, trigger and common event requirements, the selection in this search channel continues with the requirement of a Z candidate and small $E_{\mathrm{T}}^{\mathrm{miss}}$. For the reconstruction of Z candidates the events are required to have exactly two selected electrons or muons that fulfill the requirements described in Section 3. Events having additional selected leptons are rejected. The two leptons are required to be oppositely charged in the case of muons. For electrons, no such requirement is applied to minimize efficiency loss resulting from electron charge misidentification. The $m_{\ell\ell}$ distributions are shown in Figure 1. The leptonic Z decay candidates are selected by requiring the invariant mass of the two leptons to lie within the range $76 < m_{\ell\ell} < 106$ GeV (approximately ± 15 GeV around the mass of the Z boson). This strongly suppresses background from events without a real Z boson, such as $t\bar{t}$ and multijet production.

The remaining selections are:

- The signal $ZH \to \ell\ell b\bar{b}$ events are not expected to have significant $E_{\mathrm{T}}^{\mathrm{miss}}$ in contrast to background events such as those from $t\bar{t}$. Therefore a requirement of $E_{\mathrm{T}}^{\mathrm{miss}} < 50$ GeV is applied. The $E_{\mathrm{T}}^{\mathrm{miss}}$ distribution before the cut is shown in Fig. 2 (left).

- At least two jets with $p_{\mathrm{T}} > 25$ GeV are required where the two highest p_{T} jets are both required to pass the b-tagging selection. The $m_{\ell\ell}$ distribution after this requirement, but without the cut on $m_{\ell\ell}$, is shown in Fig. 2 (right). The number of $b-$tagged jets per event is shown in Fig. 3 (left). Events with two b-tagged jets are used in the analysis.

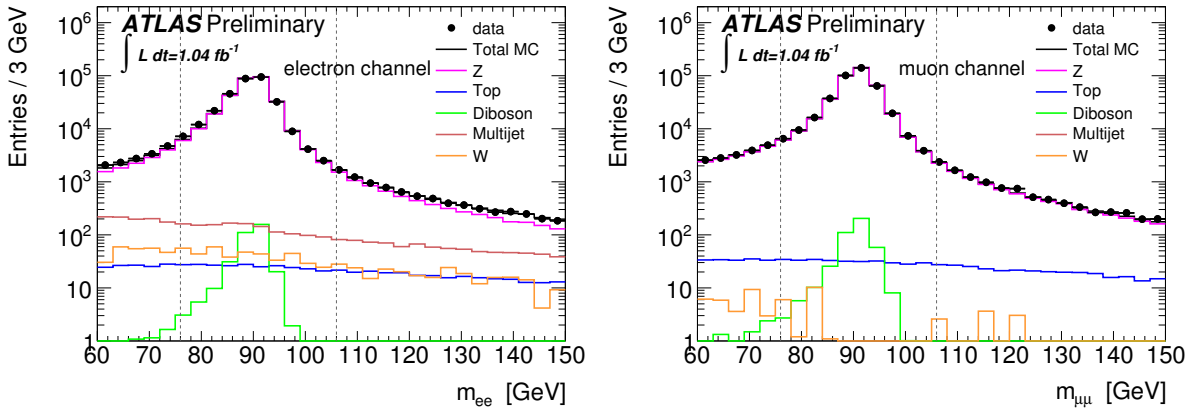

Figure 1: Distributions of $m_{\ell\ell}$ for the ZH analysis for electrons (left) and muons (right). The event selection cuts are indicated by the vertical dashed lines. The error bars in this and all subsequent figures represent the statistical uncertainty.

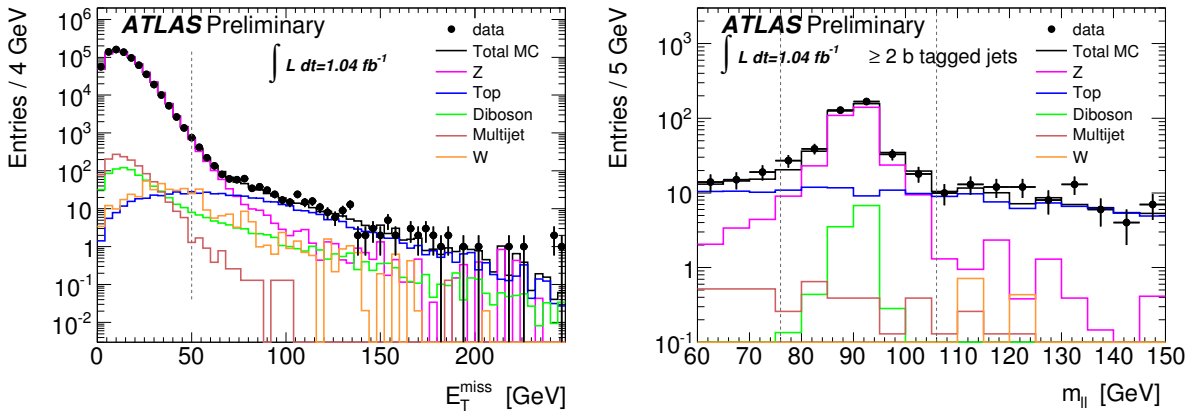

Figure 2: The distribution of $E_{\mathrm{T}}^{\mathrm{miss}}$ (left) for the $ZH \to \ell\ell b\bar{b}$ search before the $E_{\mathrm{T}}^{\mathrm{miss}}$ cut is applied. The di-lepton invariant mass ($m_{\ell\ell}$) distribution (right) after applying the low $E_{\mathrm{T}}^{\mathrm{miss}}$ cut and requiring at least two high p_{T} b-tagged jets. The event selection cuts are indicated by the vertical dashed lines.

4.3 Selection of $WH \to \ell\nu b\bar{b}$ Candidates

$WH \to \ell\nu b\bar{b}$ events are characterized by a lepton originating from a W decay and significant $E_{\mathrm{T}}^{\mathrm{miss}}$. Candidate events are therefore selected with the following criteria:

- To reduce backgrounds from processes with 2 real leptons such as from Z and $t\bar{t}$ decays, events are required to have exactly one lepton (e or μ) fulfilling the selections described above.
- The missing transverse energy $E_{\mathrm{T}}^{\mathrm{miss}}$ is required to be greater than 25 GeV to reduce background from events without large real $E_{\mathrm{T}}^{\mathrm{miss}}$ such as Z decays to leptons, when one of the leptons escapes detection, and QCD multijet background . The $E_{\mathrm{T}}^{\mathrm{miss}}$ distribution before the cut is shown in Figure 4 (top). The transverse mass, defined as $m_T = \sqrt{2p_{\mathrm{T}}^{l}p_{\mathrm{T}}^{\nu}(1-\cos(\phi^{l}-\phi^{\nu}))}$, where $p_{\mathrm{T}}^{\nu} = E_{\mathrm{T}}^{\mathrm{miss}}$ is required to be greater than 40 GeV and is shown before this cut in the lower half of Figure 4.

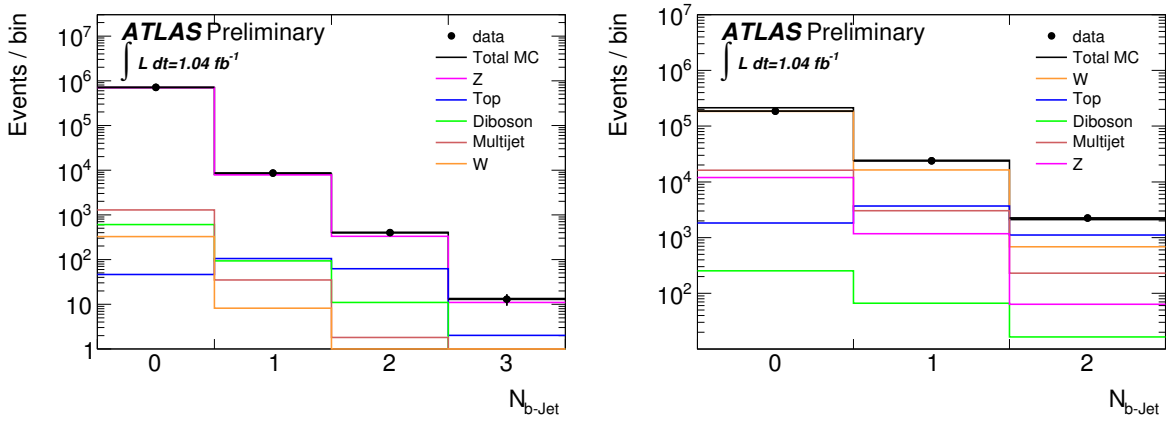

Figure 3: The distribution of the number of $b-$tagged jets per event for the $ZH \to \ell\ell b\bar{b}$ selection (left) and the $WH \to \ell\nu b\bar{b}$ selection (right). The distribution for $ZH \to \ell\ell b\bar{b}$ is shown for all events with two or more jets, whereas the distribution for $WH \to \ell\nu b\bar{b}$ is shown after the requirement of exactly two jets in the event.

- The number of jets with $p_{\mathrm{T}} > 25$ GeV is required to be exactly two to reduce background from top-quark production that is significantly higher in this channel. In addition the two jets must pass the b-tagging selection. The distribution of the number of $b-$jets per event, after the requirement on the total number of jets, is shown in Fig. 3 (right).

4.4 Search for $H \to b\bar{b}$ Decays

After the above selections for $ZH \to \ell\ell b\bar{b}$ and $WH \to \ell\nu b\bar{b}$ events, a search for $H \to b\bar{b}$ decays is performed by looking for a peak above the background expectation in the invariant mass $m_{b\bar{b}}$ of the di-b-jet system. The invariant mass is scaled by a factor of 1.05 to account for losses due to soft muons and neutrinos. The scale factor was obtained by comparing the mean of the reconstructed value of $m_{b\bar{b}}$ with the generated Higgs boson mass m_H in simulated $WH \to \ell\nu b\bar{b}$ and $ZH \to \ell\ell b\bar{b}$ samples.

5 Backgrounds to the $ZH \to \ell\ell b\bar{b}$ Search

The dominant background to the $ZH \to \ell\ell b\bar{b}$ channel is expected to be from Z+jets events, with $t\bar{t}$ production, multijet production and ZZ/WZ production also contributing. Where possible, control regions are used to determine or verify the normalization and shape of different backgrounds in the data. The control regions and data-driven evaluations of the backgrounds are very similar to, and in some cases identical to, those derived from the high mass Higgs boson search $H \to ZZ \to \ell\ell b\bar{b}$ [47], which has the same final state as the present analysis.

5.1 Z+jets Background

Measurements performed by the CDF and D0 collaborations of the Zb cross-section indicate that this cross-section, and that of the related Wb process, may not be well understood theoretically [53,54]. Due to the considerable uncertainty on the normalization of the Z+jets background a data-driven method is used to estimate it. The ALPGEN MC simulation program is used to model the shape of the $Zb\bar{b}$ contribution in the di-b-jet invariant mass $m_{b\bar{b}}$ distribution. The normalization of the simulation distribution is

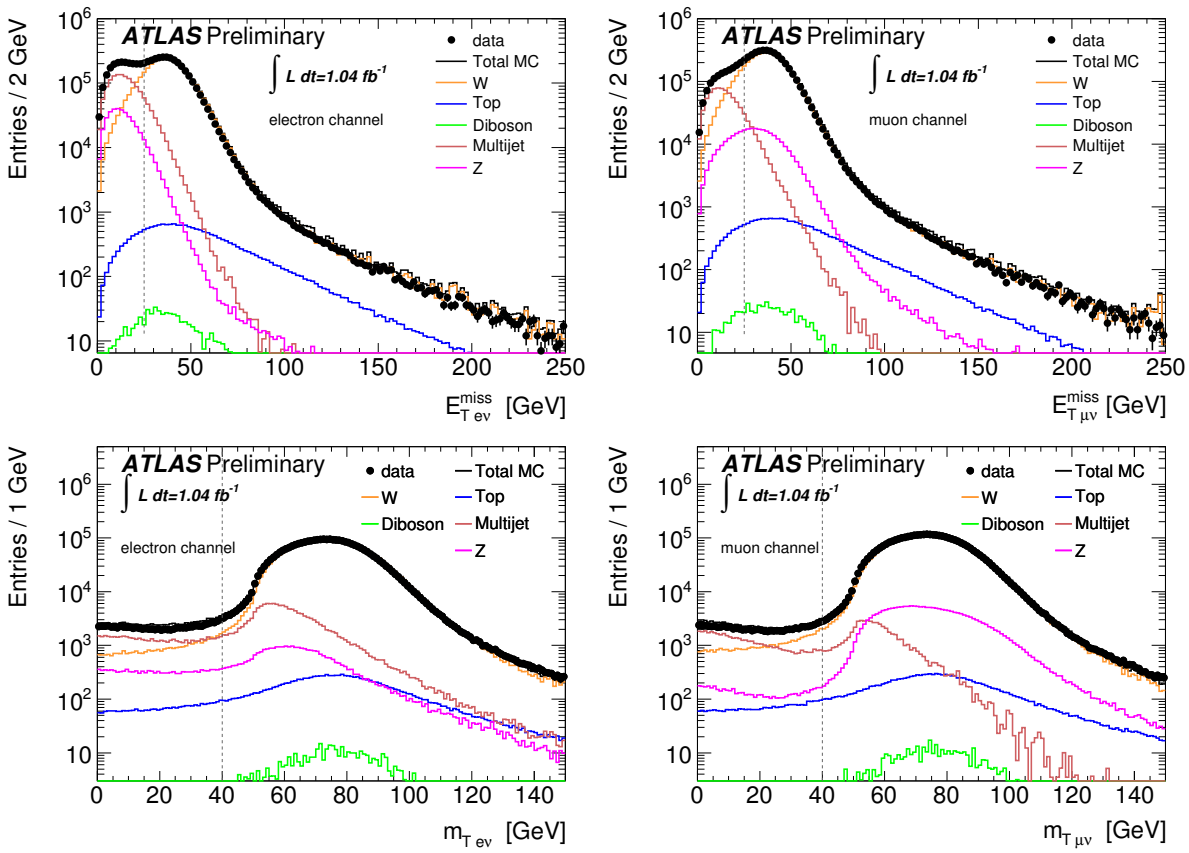

Figure 4: The distributions of $E_{\mathrm{T}}^{\mathrm{miss}}$ (top) before the cut is applied in the $WH \to \ell\nu b\bar{b}$ analysis. The distribution of the transverse mass (bottom) shown after the cut on $E_{\mathrm{T}}^{\mathrm{miss}}$. The plots are shown for electrons (left column) and muons (right column), for the WH selection. The event selection cuts are indicated by the vertical dashed lines.

determined from the $m_{b\bar{b}}$ sideband region defined by $m_{b\bar{b}} < 80$ GeV and $140 < m_{b\bar{b}} < 250$ GeV, where the $Zb\bar{b}$ background dominates (see Figure 8). In determining the number of data events to normalize the simulated sample to, the small fraction of events from non-Z+jets processes is subtracted from the data. A scale factor of 0.96 ± 0.09 is found relative to the cross-section times branching ratio given in Table 2, where the error is the statistical uncertainty only.

The normalization of the Z+jets background contribution can be cross-checked by using an extended sample where only one of the selected jets has a b-tag. The invariant mass of the two highest p_{T} jets in this case is shown in Figure 5. The normalization and shape of the data is adequately described by the MC.

5.2 ZZ Background

The Standard Model pair production of Z bosons is an irreducible background in the $ZH \to \ell\ell b\bar{b}$ search. Some of these events will survive as a peak around m_Z in the $m_{b\bar{b}}$ mass distribution. Because this background is small, and thus difficult to constrain by the data, it is taken directly from the MC simulation prediction.

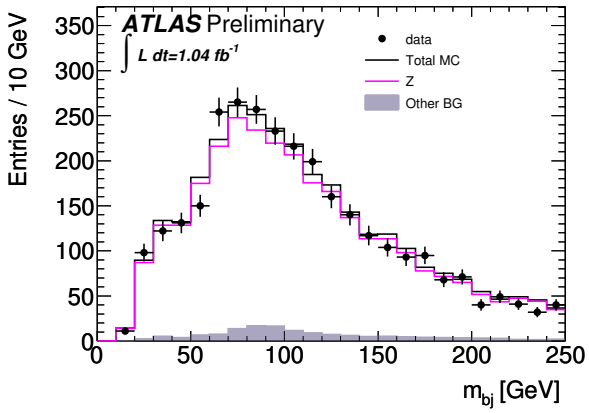

Figure 5: The invariant mass formed from the two highest p_{T} jets where only one jet is b-tagged, for the ZH analysis.

5.3 Top-quark Background

Background contributions from top-quark production, including $t\bar{t}$ and single top-quark, are estimated from the MC simulation but the normalizations are checked using a control sample in the data. Events in the control sample are required to pass the common selection described in Section 4.1, but lie in sidebands of the di-lepton mass distribution. The sidebands are defined as $60 < m_{\ell\ell} < 76$ GeV or $106 < m_{\ell\ell} < 150$ GeV. The top-quark control region is further defined by applying the standard $b-$tagging criteria as in Section 4.2. Figure 6 shows the $m_{b\bar{b}}$ distribution for data and the MC simulation background samples in this region. The distribution is seen to be dominated by top-quark production and provides an adequate description of the shape and normalization of the data within the statistical precision of the comparison.

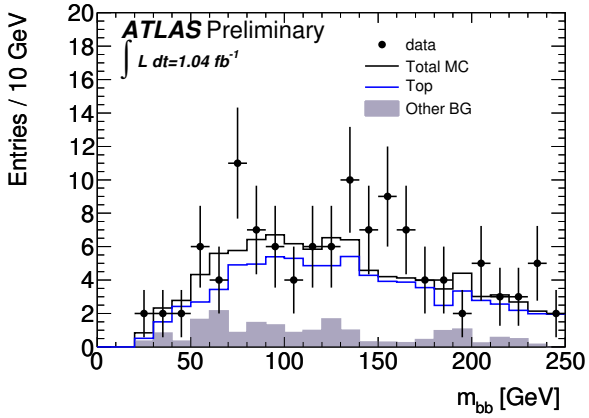

Figure 6: The invariant mass formed from two b-tagged jets, using the sidebands of the $m_{\ell\ell}$ distribution, for the ZH analysis.

5.4 QCD Multijet Background

Multijet production may form a background if the two leptons that constitute the Z boson candidate arise from particles in the jets. These particles include hadrons that are misidentified as leptons. Photon

conversions also contribute in the case of electrons, while pion decays in flight add to the muon channel. In addition, true leptons from the semileptonic decay of heavy flavour hadrons may contribute in both the electron and muon channels.

The multijet background in the electron channel is estimated from data using the template method, as described in the $H \to ZZ \to \ell\ell b\bar{b}$ analysis [19]. A multijet dominated sample is obtained from the data by selecting electrons that fail the nominal selection but pass loose identification criteria. The remaining analysis cuts are applied as before and the resulting data histograms are used as templates to describe the shape of the multijet background in the various distributions. The normalization scale factor of the multijet template is obtained with a multicomponent fit of the di-lepton invariant mass for events with at least two jets. The resulting scale factor is 0.13 ± 0.02. The scale factor obtained from a fit to the di-lepton invariant mass using events with two b-jets is found to be consistent but with this scale factor but has a large error due to low statistics. Therefore a 100% systematic uncertainty is assigned to the multijet background in the ZH analysis.

In the muon channel, the QCD multijet background is estimated from the semileptonic $b\bar{b}/c\bar{c}$ MC simulation samples and is found to be negligible after the application of the $m_{\mu\mu}$ requirement.

The resulting dielectron and dimuon mass distributions are shown in Figure 1 before any requirement on the number of jets and in Figure 2 (right) after requiring two $b-$jets in the event.

5.5 Other Backgrounds

Other backgrounds which were investigated but found to be negligible are W+jet and WW production. Top-quark pair production where both W bosons decay hadronically was also found to be negligible.

6 Backgrounds to the $WH \to \ell\nu b\bar{b}$ Search

The dominant background in the $WH \to \ell\nu b\bar{b}$ channel is $t\bar{t}$ production, with single top-quark production, QCD multijet production and W+jets also contributing significantly. Background from Z+jets and di-boson production are also considered.

6.1 Top-quark Background

The background from top-quark production, including $t\bar{t}$ and single top events, can be significantly reduced by requiring exactly two reconstructed jets as top events have, on average, a larger number of jets than the signal sample. The shape of the top-quark background, including the remaining $t\bar{t}$ contribution and the single top-quark production, is estimated from MC but the normalization is determined from a fit to the sidebands of the $m_{b\bar{b}}$ distribution. The sideband region is defined by $m_{b\bar{b}} < 80$ GeV and $140 < m_{b\bar{b}} < 250$ GeV with the top-quark and W+jets contributions being important at high and low $m_{b\bar{b}}$ respectively. The small fraction of non-top-quark and non-W+jets background is subtracted from the $m_{b\bar{b}}$ data distribution. A log-likelihood fit is performed on the subtracted data with two free parameters: (1) the normalization of the top-quark MC simulation and (2) the normalization of the $W+$ jets template (see Section 6.2). The result of the scale factor for the top-quark MC simulation from the fit to the $m_{b\bar{b}}$ sidebands is 1.22 ± 0.07.

The shape and normalization of the top-quark background may be further checked in data by examining the control region defined by the presence of three jets in the event, two of which are required to be b-jets. The di-b-jet invariant mass $m_{b\bar{b}}$ distribution for events in the top-quark control region is shown in Figure 7. A reasonable description of the normalization and shape of the data is provided by the MC, consistent within the statistical and systematic uncertainties with the scale factor derived from the fit to the sidebands of the $m_{b\bar{b}}$ distribution. ATLAS has also measured the $t\bar{t}$ production cross-section recently and the result is found to agree with theoretical predictions [55].

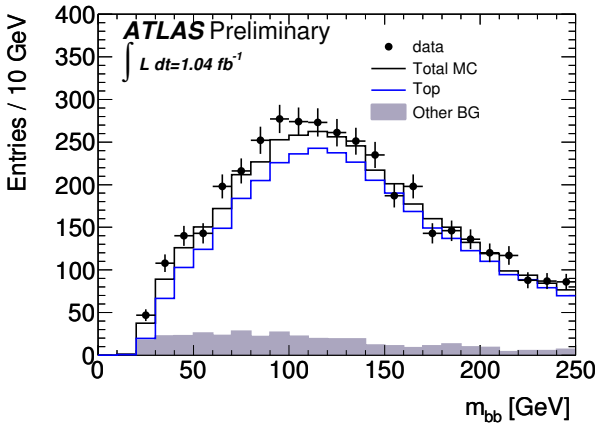

Figure 7: The di-b-jet invariant mass for the control region for top-quark events in the $WH \to \ell\nu b\bar{b}$ analysis where the requirement on the maximum number of jets is relaxed from two to three.

6.2 W+jets Background

The theoretical cross-section of the $Wb\bar{b}$ process has a considerable uncertainty and therefore a data-driven method is used to estimate it. According to the MC simulation the shape of the invariant mass m_{jj} of the untagged sample in W+jets events is consistent with the invariant mass $m_{b\bar{b}}$ when the two jets are b-tagged. Therefore, the shape of the untagged m_{jj} distribution in data is used to model the shape of the $Wb\bar{b}$ contribution. The data-driven template is evaluated by subtracting the small fraction of non-W background predicted by the MC simulation from the data m_{jj} distribution. The normalization of the template is determined from the fit to the sidebands of the $m_{b\bar{b}}$ distribution as described above in Section 6.1. The scaling factor for the m_{jj} distribution to the $m_{b\bar{b}}$ distribution is found, from the sideband fit, to be 0.00327 ± 0.00045. After normalization, the m_{jj} template plus other contributions provide a good description of the shape of the $m_{b\bar{b}}$ distribution as seen in Figure 9.

6.3 Diboson Background

The irreducible background from WZ decays, where the W boson decays to a lepton and neutrino and the Z boson to a pair of b-quarks, although much smaller than the contribution from other backgrounds, is important since it has the same final state as the signal. In this analysis it is estimated from the MC simulation. The contribution of WW production where one boson decays to a lepton and neutrino and the other W decays hadronically to two light quark jets is also estimated from the simulation.

6.4 Multijet Background

The QCD multijet background for the WH channel is evaluated in a similar way as for the ZH analysis as described in Section 5.4. The background is estimated from data for both the electron and muon channel using the template method and fitting the $E_{\mathrm{T}}^{\mathrm{miss}}$ distribution for the normalization. The QCD background dominated templates are obtained by reversing the isolation requirements in the selection of the leptons. The description of the data by the multijet background templates is investigated by defining a QCD background control region for which the $E_{\mathrm{T}}^{\mathrm{miss}}$ and M_T cuts are inverted i.e. $E_{\mathrm{T}}^{\mathrm{miss}} < 25$ GeV and $M_T < 40$ GeV but all other selections, including the b-tagging, are applied. The multijet background templates are found to provide a reasonable description of the $m_{b\bar{b}}$ distribution for this sample and a systematic error of 50% is assigned.

6.5 Other Backgrounds

The shape of the Z+jets background is modelled by the ALPGEN MC simulation. The normalization of the MC simulation is adjusted, as determined by the fit to the control region in the ZH analysis, as described in Section 5.1.

7 Systematic Uncertainties

Sources of systematic uncertainty considered were those arising from: the efficiency for reconstructing objects in the ATLAS detector, their momentum or energy resolution, the normalization and shape of the $m_{b\bar{b}}$ distribution for the signal and background processes and the luminosity measurement. The systematic uncertainties from the detector-related contributions are described briefly below and summarized in Table 3. The remaining sources of systematic error are summarized in Table 4. The effect that these uncertainties have on the signal yields are shown in Table 5.

- **Detector-related systematic uncertainties**
  The main detector-related contributions to the systematic uncertainties are from the lepton, jet and missing transverse energy reconstruction and identification efficiencies, their momentum or energy resolution and scale, the b-tagging efficiency and mis-tagging rates and the trigger efficiencies. The detector and reconstruction-related systematic uncertainties are summarized in Table 3 [43, 48, 49, 56, 57].

- **Cross-sections of Higgs boson production**
  Standard Model Higgs boson production cross-sections have been studied extensively by the LHC Higgs cross-section working group and the results are compiled in Ref. [13]. The uncertainties on these cross sections are due to variation of the factorization and renormalization scales, imperfect knowledge of the parton distribution functions (PDFs) and the uncertainty on the strong coupling constant. These uncertainties are treated according to the recommendations given in Refs. [13, 58–61] and they have been estimated to be 5% for WH and ZH in the mass range relevant for this analysis.

- ***W/Z*+jets backgrounds**
  The uncertainty on the normalization of the Z+jets background for both the ZH and WH analyses is 9%, taken from the statistical uncertainty on the data-driven method obtained from the Z+jets control regions in the ZH analysis (see Section 5.1). A further uncertainty due to the shape of the Z+jets distribution in the ZH analysis is estimated by replacing the ALPGEN Monte Carlo prediction by that from PYTHIA. To avoid adding an extra normalization systematic, the final distribution from the PYTHIA prediction is scaled to have the same number of events as that of the ALPGEN MC sample.

  A normalization uncertainty of 14% is assigned to the W+jets background based on the statistical precision of the data-driven normalization method (see Section 6.2). An uncertainty on the shape of the W+jets contribution is estimated by replacing the data-driven background template with that derived from the ALPGEN Monte Carlo. A further uncertainty on the shape is estimated by replacing the W+jets template with that in which the dijet mass m_{jj} is scaled by 1.05 since the dijet mass in tagged events $m_{b\bar{b}}$ is scaled by this factor (see Section 4.4).

- **Top-quark background**
  The normalization error for the top background determined using the Monte Carlo is taken to be 9% for the ZH analysis, from comparisons of data and MC simulation in the control region

(Section 5.3), and 6% for the WH analysis from the statistical precision of the data-driven normalization determination (Section 6.1).

- **Diboson background**
  For the ZH analysis the largely irreducible Standard Model ZZ background, where the definition of an effective control region is difficult, is taken directly from the Monte Carlo. A systematic error based on a 5% combined scale and PDF uncertainty for the NLO cross-section is convolved with a further 10% error, corresponding to the maximum difference seen in the comparisons between the k-factor scaled PYTHIA and the MC@NLO results. This leads to an overall 11% error on the normalization. The relatively small WZ background is also taken directly from the Monte Carlo with an assumed normalization error of 11%, identical to that for the ZZ background.

  For the WH analysis the normalizations of the irreducible diboson background from WZ and the background from WW production are taken from Monte Carlo. A theoretical uncertainty of 11% is applied for both processes.

- **Multijet background**
  The normalization uncertainty for the multijet background is taken to be 100% for ZH (see Section 5.4) and 50% for WH (see Section 6.4).

- **Luminosity**
  The uncertainty in the integrated luminosity has been estimated to be 3.7% [62]. This uncertainty is only applied to MC samples for which the normalization error is not taken directly from a comparison between data and MC. Where it is applied, this systematic uncertainty is assumed to be correlated across samples.

The detector-related systematics are treated as correlated between the signal and backgrounds channels and between the ZH and WH searches. For those backgrounds where the normalization is determined directly from a comparison of the $m_{b\bar{b}}$ distribution in data and MC, the detector-related errors are treated as shape systematics. The normalization uncertainties on the backgrounds are treated as correlated between the ZH and WH searches, except for the multijet normalization.

Source of Uncertainty	Treatment in analysis
Jet Energy Scale (JES)	$2-7\%$ as a function of p_{T} and η
Jet Pile-up Uncertainty	$2-7\%$ as a function of p_{T} and η
b-quark Energy Scale	2.5%
Jet Energy Resolution	$5-12\%$
Electron Selection Efficiency	$0.7-3\%$ as a function of p_{T}, $0.4-6\%$ as a function of η
Electron Trigger Efficiency	$0.4-1\%$ as a function of η
Electron Reconstruction Efficiency	$0.7-1.8\%$ as a function of η
Electron Energy Scale	$0.1-6\%$ as a function of η, pileup, material effects etc.
Electron Energy Resolution	Sampling term 20%, a small constant term has a large variation with η
Muon Selection Efficiency	$0.2-3\%$ as a function of p_{T}
Muon Trigger Efficiency	$< 1\%$
Muon Momentum Scale	$2-16\%$ η-dependent systematic on scale
Muon Momentum Resolution	p_{T} and η-dependent resolution smearing functions, systematic $\leq 1\%$
b-tagging Efficiency	$5-14\%$ as a function of p_{T}
b-tagging Mis-tag Fraction	$8-12\%$ as a function of p_{T} andη
Missing Transverse Energy	Add/subtract object uncertainties in $E_{\mathrm{T}}^{\mathrm{miss}}$

Table 3: Sources of detector and reconstruction-related systematic uncertainties.

Source of Uncertainty	Treatment in analysis	
	ZH	WH
Luminosity	3.7%	3.7%
Higgs boson cross-section	5%	5%
Background norm. and shape:		
Top	9%	6%
Z+jets	9% plus shape	9%
W+jets	negligible	14% plus shapes
ZZ	11%	negligible
WZ	11%	11%
WW	negligible	11%
QCD multijets	100%	50%

Table 4: Sources of non-detector-related systematic uncertainties.

Source of Uncertainty	Effect on $ZH \to \ell\ell b\bar{b}$ signal		Effect on $WH \to \ell\nu b\bar{b}$ signal	
	m_H = 115 GeV	m_H = 130 GeV	m_H = 115 GeV	m_H = 130 GeV
Electron Energy Scale	< 1%	< 1%	1%	1%
Electron Energy Resolution	< 1%	< 1%	1%	1%
Muon Momentum Resolution	1%	3%	4%	1%
Jet Energy	9%	7%	1%	3%
Jet Energy Resolution	< 1%	< 1%	1%	1%
Missing Transverse Energy	2%	2%	2%	3%
b-tagging Efficiency	16%	17%	16%	17%
b-tagging Mis-tag Fraction	< 1%	< 1%	3%	3%
Electron Efficiency	1%	1%	1%	1%
Muon Efficiency	1%	1%	1%	1%
Luminosity	4%	4%	4%	4%
Higgs Cross-section	5%	5%	5%	5%

Table 5: Effect of the different systematic uncertainties on the signal yields for the $ZH \to \ell\ell b\bar{b}$ and $WH \to \ell\nu b\bar{b}$ channels, for two different Higgs boson masses. Here *Jet Energy* refers to jet energy scale, pile-up and b-jet energy scale uncertainties; *Electron Efficiency* to trigger, reconstruction and selection efficiencies and *Muon Efficiency* refers to the muon trigger and selection efficiencies.

8 Results

Tables 6 and 7 summarize the numbers of estimated background events and observed events in data for the ZH and WH analyses. Also shown are expected signal yields for each channel for several representative Higgs boson masses.

Source	expected events		(stat.)		(sys.)
Z+jets	261.0	±	7.8	±	24.6
Top-quark	52.0	±	1.3	±	10.6
Multijet	1.4	±	0.4	±	1.4
ZZ	9.2	±	1.1	±	2.3
WZ	1.1	±	0.3	±	0.3
Total background	324.7	±	8.0	±	27.9
Data	329				
Signal m_H = 110 GeV	2.22	±	0.09	±	0.43
Signal m_H = 115 GeV	1.91	±	0.07	±	0.38
Signal m_H = 120 GeV	1.58	±	0.06	±	0.32
Signal m_H = 125 GeV	1.44	±	0.05	±	0.28
Signal m_H = 130 GeV	1.02	±	0.04	±	0.20

Table 6: Summary of numbers of the estimated background events, observed events in data, and expected signal yields for the ZH analysis. Electron and muon channels are combined. The statistical and systematic uncertainties on the estimated background and signal events are also shown.

Source	expected events		(stat.)		(sys.)
Z+jets	54.4	±	3.9	±	12.3
W+jets	466.7	±	1.4	±	66.5
Top-quark	1141.8	±	8.8	±	78.0
Multijet	193.0	±	9.4	±	96.5
WZ	16.1	±	2.2	±	3.4
WW	4.8	±	1.1	±	1.4
Total background	1876.8	±	13.7	±	147.2
Data	1888				
Signal m_H = 110 GeV	6.72	±	0.31	±	1.20
Signal m_H = 115 GeV	5.25	±	0.30	±	0.97
Signal m_H = 120 GeV	4.54	±	0.25	±	0.83
Signal m_H = 125 GeV	4.08	±	0.21	±	0.77
Signal m_H = 130 GeV	3.28	±	0.17	±	0.62

Table 7: Summary of numbers of the estimated background events, observed events in data, and expected signal yields for the WH analysis. Electron and muon channels are combined. The statistical and systematic uncertainties on the estimated background and signal events are also shown.

The analysis is performed for five Higgs boson masses between 110 GeV and 130 GeV. The di-b-jet invariant mass $m_{b\bar{b}}$ is shown in Figure 8 for $ZH \to \ell\ell b\bar{b}$ and in Figure 9 for $WH \to \ell\nu b\bar{b}$, for two example Higgs boson masses, m_H = 115 and 130 GeV. The data distributions are overlaid with the expectations from the MC simulation and data-driven backgrounds. The background expectation agrees well with the data.

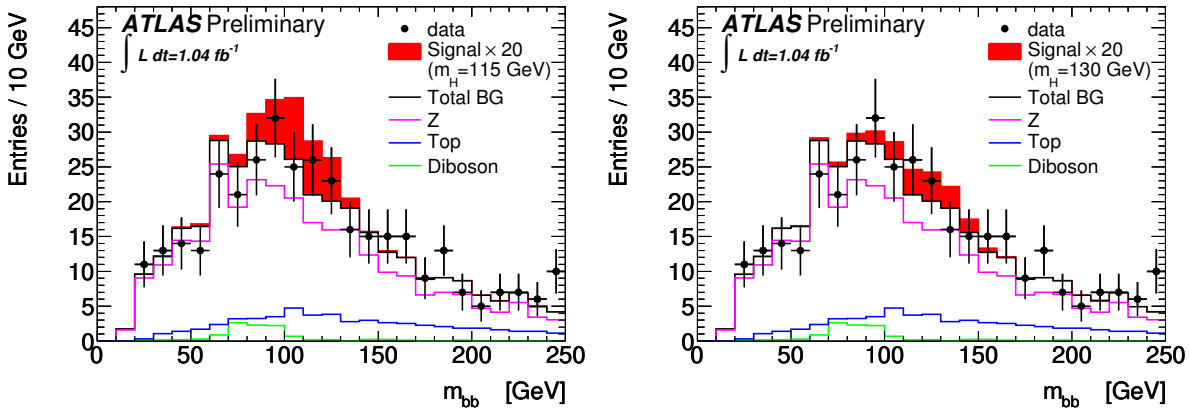

Figure 8: The invariant mass, $m_{b\bar{b}}$, for $ZH \to \ell\ell b\bar{b}$ for $m_H = 115$ (left) and 130 GeV (right). The signal distribution is enhanced by a factor of 20 for visibility.

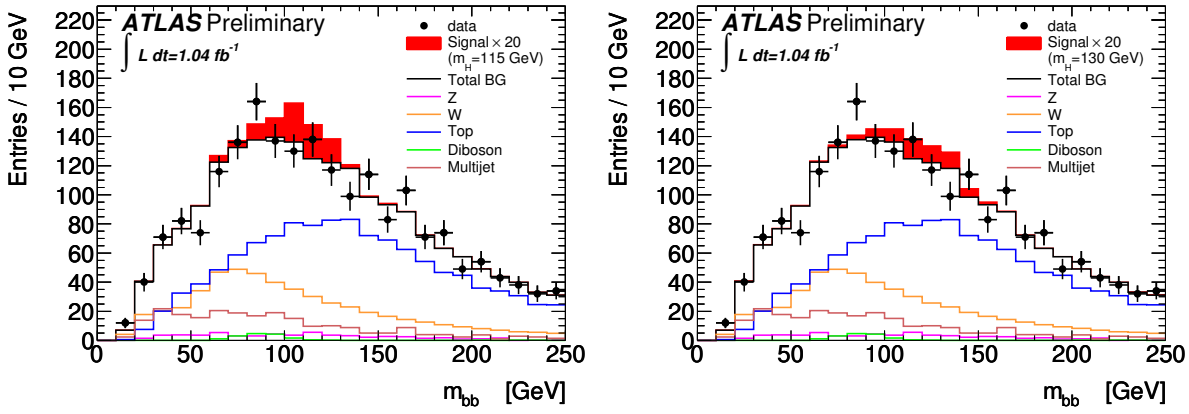

Figure 9: The invariant mass, $m_{b\bar{b}}$, for $WH \to \ell\nu b\bar{b}$ for $m_H = 115$ (left) and 130 GeV (right). The signal distribution is enhanced by a factor of 20 for visibility.

For each Higgs boson mass hypothesis a one-sided upper-limit is placed on the standardized cross-sections $\mu = \sigma/\sigma_{SM}$ at the 95% confidence level (C.L.). The exclusion limits are derived from the CL_s [63] treatment of the p-values computed with the profile likelihood ratio [64], as implemented in the RootStats program [65], of the binned distribution of $m_{b\bar{b}}$ as the test-statistic. The systematic uncertainties are treated as nuisance parameters and shape uncertainties are treated in the limit program via morphing.

The resulting exclusion limits can be seen in Figure 10, for the ZH and WH analysis. The limits range between 15 and 30 times the Standard Model cross-section for the $WH \to \ell\nu b\bar{b}$ channel and between 15 and 35 times the Standard Model cross-section for the $ZH \to \ell\ell b\bar{b}$ channel, depending on the Higgs boson mass. The combined exclusion limit for both channels together, shown in Figure 11, ranges between 10 to 20 times the Standard Model cross-section, depending on the Higgs boson mass.

As the number of events in the selected sample was sufficiently large, analytic expressions that are exact in the large-sample limit [64] were employed to describe the sampling distribution of the test statistic used in the exclusion limit calculation. This has the advantage of being computationally far faster than generating many toy Monte Carlo experiments.

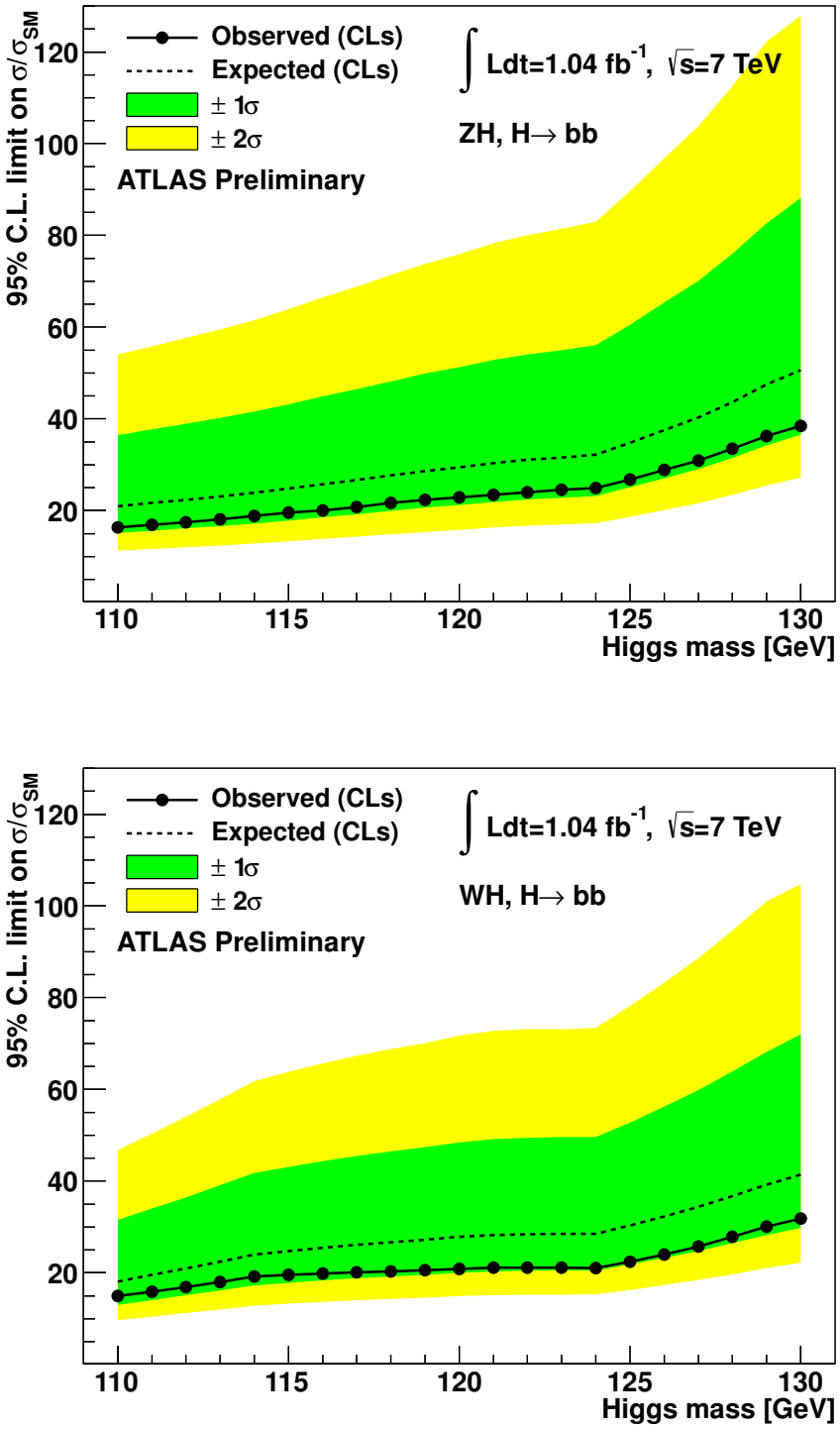

Figure 10: Expected (dashed) and observed (solid line) exclusion limits for the $ZH \to \ell\ell b\bar{b}$ (top) and $WH \to \ell\nu b\bar{b}$ (bottom) channels expressed as the ratio to the Standard Model cross-section, using the profile-likelihood method with CL_s. The green and yellow areas represent the 1σ and 2σ ranges of the expectation in the absence of a signal.

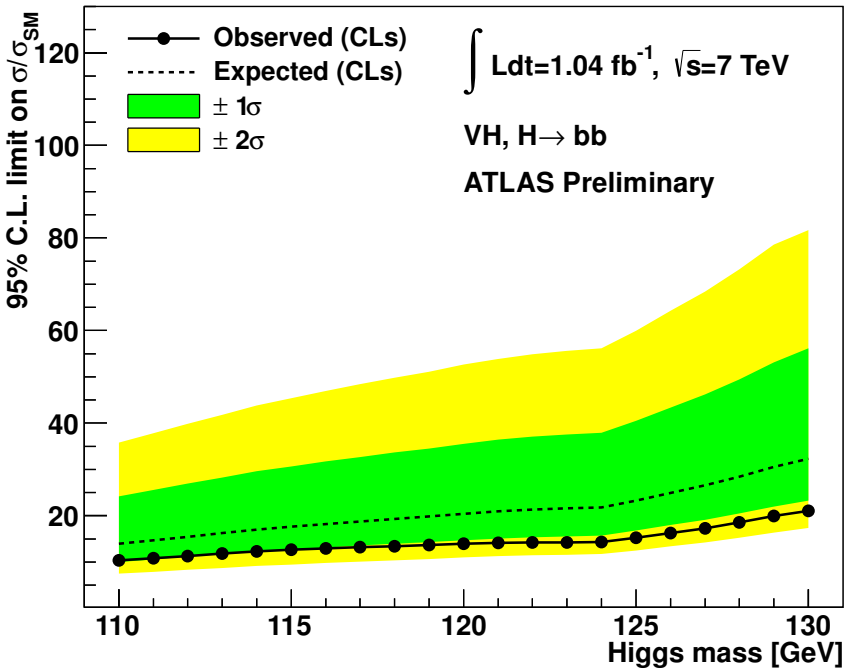

Figure 11: Expected (dashed) and observed (solid line) exclusion limits for the $ZH \rightarrow \ell\ell b\bar{b}$ and $WH \rightarrow \ell\nu b\bar{b}$ channels combined, expressed as the ratio to the Standard Model cross-section, using the profile-likelihood method with CL_s. The green and yellow areas represent the 1σ and 2σ ranges of the expectation in the absence of a signal.

9 Boosted WH Studies

An alternative approach to identifying $H \to b\bar{b}$ in associated production with a W or Z boson is to consider only the high-p_{T} part of the cross-section [18,66]. Such "boosted" studies require that the Higgs boson p_{T} is at least 200 GeV, which rejects about 95% of the signal. However the main backgrounds are reduced by a larger factor and the remaining signal events tend to be within the detector acceptance.

One of the key aspects of any such analysis is the identification of the $H \to b\bar{b}$ pair. The Higgs boson system has a few useful properties which can be exploited. Firstly, as the Higgs boson p_{T} increases, the angle between the $b\bar{b}$ pair decreases. The b and $\bar{b}$-jets in the $b\bar{b}$ pair will tend to share the available p_{T} roughly equally, which is not the case for $g \to b\bar{b}$ splittings. Although the b-quarks may produce additional radiation through further splittings, due to angular ordering [67–69] this should be emitted at angles smaller than the angle between the b-quarks themselves.

For highly boosted $H \to b\bar{b}$, it is found that "jet substructure" techniques offer significant advantages over traditional jet reconstruction. Specifically a procedure is employed where Cambridge-Aachen [70, 71] R=1.2 jets are built by combining their constituent four-vectors, and the jet mass at each combination is recorded. The clustering history is then searched in reverse for a step where the mass of the jet falls by more than 1/3 in a fairly symmetric manner. At this point the remaining constituents are reclustered using a smaller R value and the three highest p_{T} "subjets" are taken to form a heavy particle candidate, with irrelevant radiation filtered out. The subjets are then examined by a b-tagging algorithm to reject light jet backgrounds. The mass of this new split and filtered jet is the final discriminating variable, analogous to the dijet mass.

Overall, the loss of available data statistics in this approach is found to be compensated by an improvement in signal-to-background ratio [72]. However, this method presents challenges, as jet substructure procedures are relatively unexplored in collision data. It is therefore important to understand whether the substructure properties of jets are well modelled by Monte Carlo generators and the detector simulation. Initial indications are that this particular procedure is well understood at ATLAS [73].

Figure 12 takes a first look at the mass distribution for these split and filtered jets with no b-tagging applied. First, events are selected if they contain a $W \to \ell\nu$ candidate consistent with having a boson $p_{\mathrm{T}} > 200$ GeV. Then all split and filtered jets with $p_{\mathrm{T}} > 180$ GeV and $\Delta\phi_{W,jet} > 1.2$ in these events are studied. The jet mass distribution in a sample of 2011 data is compared to MC simulation. There are three main backgrounds: $t\bar{t}$ events were generated with MC@NLO [33, 74] with Herwig [32, 75] and Jimmy [34] for parton showers; W+jets with Alpgen [31] also interfaced with Herwig and Jimmy for parton showers and WW production with Herwig and Jimmy. All samples are normalized to the highest order cross-section calculation available (see Table 2). A jet calibration derived from simulated QCD jets is applied but no correction for the specific environment of these events is applied. No corrections are applied to MC simulated events nor are any systematic uncertainties evaluated.

In spite of the raw nature of the comparison, the mass distribution is reasonably well described by MC simulation. It is also interesting to note the excess in both data and MC simulation around the W-boson mass. This implies that this may be an extremely useful control sample for controlling systematics in a final analysis.

These first results are encouraging, promising new results from the boosted jet substructure analysis in the near future.

10 Summary

This note summarizes the results of the first ATLAS direct search for the Standard Model Higgs boson in the mass range $110 < m_H < 130$ GeV when produced in association with a W or Z boson and decaying to $b\bar{b}$. The analysis uses a dataset corresponding to 1.04 fb^{-1} of pp collisions at $\sqrt{s} = 7$ TeV. No significant

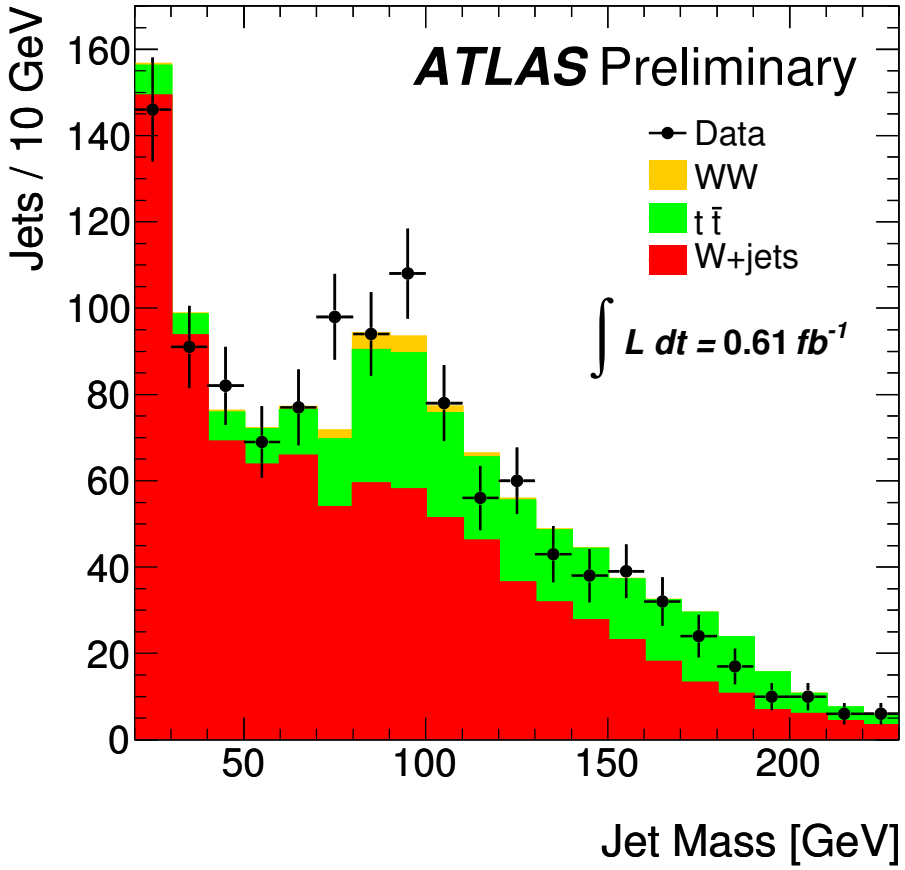

Figure 12: The jet mass distribution of subjets with $p_{\mathrm{T}} > 180$ GeV in events consistent with a $W \to \ell\nu$ boson decay with $p_{\mathrm{T}} > 200$ GeV. The distribution is compared to the uncorrected MC simulation prediction for $t\bar{t}$, W+jets and WW processes.

excess of events above the estimated backgrounds is observed. Upper limits on Higgs boson production, at the 95% confidence level, of 10 to 20 times the Standard Model cross-section are obtained in the mass range between 110 and 130 GeV.

The first study in ATLAS of the background to the search for highly boosted Higgs bosons decaying to $b\bar{b}$ pairs, based on an analysis of jet substructure, shows promising results.

References

[1] S. L. Glashow, *Partial Symmetries of Weak Interactions*, Nucl. Phys. B **22** (1961) 579.

[2] S. Weinberg, *A Model of Leptons*, Phys. Rev. Lett. **19** (1967) 1264.

[3] A. Salam, *Elementary Particle Theory*. Almqvist and Wiksells, Stockholm, 1968.

[4] F. Englert and R. Brout, *Broken Symmetry and the Mass of Gauge Vector Mesons*, Phys. Rev. Lett. **13** (1964) 321.

[5] P. W. Higgs, *Broken symmetries, massless particles and gauge fields*, Phys. Lett. **12** (1964) 132.

[6] P. W. Higgs, *Broken Symmetries and the Masses of Gauge Bosons*, Phys. Rev. Lett. **13** (1964) 508.

[7] G. Guralnik, C. Hagen, and T. Kibble, *Global conservation laws and massless particles*, Phys. Rev. Lett. **13** (1964) 585–587.

[8] P. W. Higgs, *Spontaneous Symmetry Breakdown without Massless Bosons*, Phys. Rev. **145** (1966) 1156.

[9] T. Kibble, *Symmetry breaking in non-Abelian gauge theories*, Phys. Rev. **155** (1967) 1554–1561.

[10] O. S. Bruning (Ed.) et al., *LHC Design Report. 1. The LHC main ring*, CERN-2004-003-V-1 .

[11] O. S. Buning (Ed.) et al., *LHC Design Report. 2. The LHC infrastructure and general services*, CERN-2004-003-V-2 .

[12] M. Benedikt, (Ed.), P. Collier, (Ed.), V. Mertens, (Ed.), J. Poole, (Ed.), and K. Schindl, (Ed.), *LHC Design Report. 3. The LHC injector chain*, CERN-2004-003-V-3 .

[13] LHC Higgs Cross Section Working Group, S. Dittmaier, C. Mariotti, G. Passarino, and R. Tanaka (Eds.), *Handbook of LHC Higgs cross sections: 1. Inclusive observables*, CERN-2011-002 (CERN, Geneva, 2011) , arXiv:1101.0593 [hep-ph].

[14] D0 Collaboration, *Search for WH associated production with 5.3 fb^{-1} of Tevatron data*, D0 Note 6092-Conf (2010) .

[15] D0 Collaboration, *A Search for $ZH \to \ell^+\ell^- b\bar{b}$ Production in 6.2 fb^{-1} of data with the D0 detector in $p\bar{p}$ collisions at $\sqrt{s}$ = 1.96 TeV*, D0 Note 6089-Conf (2010) .

[16] CDF Collaboration, *Search for Standard Model Higgs Boson Production in Association with a W Boson using Neural Networks with 5.7 fb^{-1} of CDF data*, CDF/PUB/EXOTIC/PUBLIC/10239 (2010) .

[17] CDF Collaboration, *A Search for the Standard Model Higgs boson in the process $ZH \to \ell^+\ell^- b\bar{b}$ using 5.7 fb^{-1} of CDF II Data* , CDF Note 10235-Conf (2010) .

[18] ATLAS Collaboration, *ATLAS Sensitivity to the Standard Model Higgs in the HW and HZ Channels at High Transverse Momenta*, ATL-PHYS-PUB-2009-088 (2009) .

[19] ATLAS Collaboration, *Search for a Standard Model Higgs Boson in the Mass Range 200-600 GeV in the Channels $H \to ZZ \to \ell\ell\nu\nu$ and $H \to ZZ \to \ell\ell qq$ with the ATLAS Detector*, ATLAS-CONF-2011-026 (2011) .

[20] ATLAS Collaboration, *The ATLAS Experiment at the CERN Large Hadron Collider*, JINST **3** (2008) S08003.

[21] ATLAS Collaboration, G. Aad et al., *The ATLAS Simulation Infrastructure*, Eur. Phys. J. C **70** (2010) 823–874, arXiv:1005.4568 [physics.ins-det].

[22] S. Agostinelli et al., *GEANT4: A simulation toolkit*, Nucl. Instrum. Meth. A **506** (2003) 250–303.

[23] ATLAS Collaboration, *Luminosity Determination in pp Collisions at* $\sqrt{s} = 7$ *TeV Using the ATLAS Detector at the LHC*, arXiv:1101.2185 [hep-ex].

[24] T. Sjostrand, S. Mrenna, and P. Z. Skands, PYTHIA *6.4 Physics and Manual*, JHEP **05** (2006) 026, arXiv:hep-ph/0603175.

[25] P. Golonka and Z. Was, *PHOTOS Monte Carlo: a precision tool for QED corrections in Z and W decays*, Eur. Phys. J. C **45** (2006) 97–107, arXiv:hep-ph/0506026.

[26] Z. Was, *TAUOLA the library for tau lepton decay, and KKMC/KORALB/KORALZ/... status report*, Nucl. Phys. Proc. Suppl. **98** (2001) 96–102, arXiv:hep-ph/0011305.

[27] O. Brein, A. Djouadi, and R. Harlander, *NNLO QCD corrections to the Higgs-strahlung processes at hadron colliders*, Phys. Lett. **B579** (2004) 149–156.

[28] M. L. Ciccolini, S. Dittmaier, and M. Krämer, *Electroweak radiative corrections to associated WH and ZH production at hadron colliders*, Phys. Rev. **D68** (2003) 073003.

[29] A. Djouadi, J. Kalinowski, and M. Spira, *HDECAY: A program for Higgs boson decays in the Standard Model and its supersymmetric extension*, Comput. Phys. Commun. **108** (1998) 56–74.

[30] Particle Data Group Collaboration, K. Nakamura, *Review of particle physics*, J. Phys. G **37** (2010) 075021.

[31] M. L. Mangano et al., ALPGEN*, a generator for hard multi-parton processes in hadronic collisions*, JHEP **07** (2003) 001.

[32] G. Corcella et al., HERWIG *6: an event generator for hadron emission reactions with interfering gluons (including super-symmetric processes)* , JHEP **01** (2001) 010.

[33] S. Frixione and B. R. Webber, *Matching NLO QCD computations and parton shower simulations*, JHEP **06** (2002) 029, arXiv:hep-ph/0204244.

[34] J. M. Butterworth, J. R. Forshaw, and M. H. Seymour, *Multiparton interactions in photoproduction at HERA*, Z. Phys. C **72** (1996) 637–646, arXiv:hep-ph/9601371.

[35] Binoth, T. and Ciccolini, M. and Kauer, N. and Krämer, M., *Gluon-induced W-boson pair production at the LHC*, JHEP **12** (2006) 046, hep-ph/0611170v1.

[36] J. M. Campbell and R. K. Ellis, *An update on vector boson pair production at hadron colliders*, Phys. Rev. D **60** (1999) 113006, arXiv:hep-ph/9905386.

[37] T. Binoth, N. Kauer, and P. Mertsch, *Gluon-induced QCD corrections to* $pp \to ZZ \to \ell\bar{\ell}\ell'\bar{\ell}'$, arXiv:0807.0024 [hep-ph].

[38] K. Melnikov and F. Petriello, *Electroweak gauge boson production at hadron colliders through* $O(\alpha_s^2)$, Phys. Rev. D **74** (2006) 114017, arXiv:hep-ph/0609070.

[39] K. Melnikov and F. Petriello, *The W boson production cross section at the LHC through $O(\alpha_s^2)$*, Phys. Rev. Lett. **96** (2006) 231803, arXiv:hep-ph/0603182.

[40] S. Catani, L. Cieri, G. Ferrera, D. de Florian, and M. Grazzini, *Vector boson production at hadron colliders: a fully exclusive QCD calculation at NNLO*, Phys. Rev. Lett. **103** (2009) 082001, arXiv:0903.2120 [hep-ph].

[41] M. Aliev et al., – *HATHOR – HAdronic Top and Heavy quarks crOss section calculatoR*, arXiv:1007.1327 [hep-ph].

[42] ATLAS Collaboration, *Measurement of the $W \to \ell\nu$ and $Z/\gamma* \to \ell\ell$ production cross sections in proton-proton collisions at $\sqrt{s} = 7$ TeV with the ATLAS detector*, JHEP **12** (2010) 060, arXiv:1010.2130 [hep-ex].

[43] ATLAS Collaboration, *Expected electron performance in the ATLAS experiment*, ATLAS-PHYS-PUB-2011-006 (2011) .

[44] ATLAS Collaboration, *Muon Performance in Minimum Bias pp Collision Data at $\sqrt{s} = 7$ TeV with ATLAS*, ATLAS-CONF-2010-036 (2010) .

[45] ATLAS Collaboration, *Measurement of inclusive jet and dijet cross sections in proton-proton collisions at 7 TeV centre-of-mass energy with the ATLAS detector*, Eur. Phys. J. C **71** (2011) 1512, arXiv:1009.5908 [hep-ex].

[46] M. Cacciari, G. P. Salam, and G. Soyez, *The anti-k_t jet clustering algorithm*, JHEP **04** (2008) 063, arXiv:0802.1189 [hep-ph].

[47] ATLAS Collaboration, *Search for a Standard Model Higgs in the mass range 200-600 GeV in the channel $H \to ZZ \to \ell^+\ell^- q\bar{q}$*, ATL-COM-PHYS-2011-740 (2011) .

[48] ATLAS Collaboration, *Performance of the Missing Transverse Energy Reconstruction and Calibration in pp Collisions at Center-of-Mass Energy of $\sqrt{s} = 7$ TeV with the ATLAS Detector*, ATLAS-CONF-2011-080 (2010) .

[49] ATLAS Collaboration, *Commissioning of the ATLAS high-performance b-tagging algorithms in the 7 TeV collision data*, ATLAS note ATLAS-CONF-2011-102, CERN, Geneva, Jul, 2011.

[50] ATLAS Collaboration, *Muon reconstruction efficiency in reprocessed 2010 LHC proton-proton collision data recorded with the ATLAS detector*, ATLAS-CONF-2011-063.

[51] ATLAS Collaboration, *Muon Momentum Resolution in First Pass Reconstruction of pp Collision Data Recorded by ATLAS in 2010*, ATLAS-CONF-2011-046 (2010) .

[52] ATLAS Collaboration, *Performance of the missing transverse energy reconstruction in pp collisions at center-of-mass energy of $\sqrt{s} = 7$ GeV with the ATLAS detector*, ATLAS-CONF-2010-039.

[53] CDF Collaboration, T. Aaltonen et al., *Search for New Physics with a Dijet Plus Missing Et Signature in p anti-p Collisions at $\sqrt{s} = 1.96$ TeV*, Phys. Rev. Lett. **104** (2010) 131801.

[54] CDF Collaboration, T. Aaltonen et al., *Measurement of Cross Sections for b Jet Production in Events with a Z Boson in p-anti-p Collisions at s**(1/2) = 1.96-TeV.*, Phys. Rev. D **79** (2009) 052008.

[55] ATLAS Collaboration, *Measurement of the top quark-pair production cross section with ATLAS in pp collisions at* $\sqrt{s}$ = 7 TeV, arXiv:1012.1792 [hep-ex].

[56] ATLAS Collaboration, *Jet energy scale and its systematic uncertainty in proton-proton collisions at* $\sqrt{s}$ = 7 *TeV in ATLAS 2010 data*, Tech. Rep. ATLAS-CONF-2010-056, CERN, Geneva, July, 2010.

[57] ATLAS Collaboration, *Jet Energy Resolution and Selection Efficiency Relative to Track Jets from In-situ Techniques with the ATLAS Detector Using Proton-Proton Collisions at a Center of Mass Energy* $\sqrt{s}$ = 7 *TeV*, Tech. Rep. ATLAS-CONF-2010-054, CERN, Geneva, July, 2010.

[58] M. Botje, J. Butterworth, A. Cooper-Sarkar, A. de Roeck, J. Feltesse, et al., *The PDF4LHC working group interim recommendations*, arXiv:1101.0538 [hep-ph].

[59] H.-L. Lai, M. Guzzi, J. Huston, Z. Li, P. M. Nadolsky, et al., *New parton distributions for collider physics*, Phys.Rev. **D82** (2010) 074024, arXiv:1007.2241 [hep-ph].

[60] A. D. Martin, W. J. Stirling, R. S. Thorne, and G. Watt, *Parton distributions for the LHC*, Eur. Phys. J. **C63** (2009) 189–285, arXiv:0901.0002 [hep-ph].

[61] R. D. Ball, V. Bertone, F. Cerutti, L. Del Debbio, S. Forte, et al., *Impact of heavy quark masses on parton distributions and LHC phenomenology*, Nucl.Phys. **B849** (2011) 296–363, arXiv:1101.1300 [hep-ph].

[62] ATLAS Collaboration, *Updated Luminosity Determination in pp Collisions at* $\sqrt{s}$ = *7 TeV using the ATLAS Detector*, ATLAS-CONF-2011-011 (2011) .

[63] A. L. Read, *Presentation of search results: the* CL_s *technique*, J. Phys. G **28** (2002) 2693–2704.

[64] G. Cowan, K. Cranmer, E. Gross, and O. Vitells, *Asymptotic formulae for likelihood-based tests of new physics*, Eur. Phys. J. C **71** (2011) 1554, arXiv:1007.1727v2.

[65] L. Moneta et al., *The RooStats Project*, in *Proceedings of the 13th International Workshop on Advanced Computing and Analysis Techniques in Physics Research, ACAT2010*, Proceedings of Science. 2010. arXiv:1009.1003.

[66] J. M. Butterworth, A. R. Davison, M. Rubin, and G. P. Salam, *Jet substructure as a new Higgs search channel at the LHC*, Phys. Rev. Lett. **100** (2008) 242001, arXiv:0802.2470 [hep-ph].

[67] Mueller, A H Phys. Lett. B **104** (1981) 161.

[68] Ermolaev, B I and Fadin, V S Phys. Rept. **100** (1983) 201.

[69] Bassetto, A. and Ciafaloni, M and Marchesini, G JETP Lett. **33** (1981) 269.

[70] Y. L. Dokshitzer, G. D. Leder, S. Moretti, and B. R. Webber, *Better Jet Clustering Algorithms*, JHEP **08** (1997) 001, arXiv:hep-ph/9707323.

[71] M. Wobisch and T. Wengler, *Hadronization corrections to jet cross sections in deep- inelastic scattering*, arXiv:hep-ph/9907280.

[72] ATLAS Collaboration, *ATLAS Sensitivity Prospects for 1 Higgs Boson Production at the LHC Running at 7, 8 or 9 TeV*, Tech. Rep. ATL-PHYS-PUB-2010-015, CERN, Geneva, Nov, 2010.

[73] ATLAS Collaboration, *Measurement of Jet Mass and Substructure for Inclusive Jets in s = 7 TeV pp Collisions with the ATLAS Experiment*, Tech. Rep. ATLAS-CONF-2011-073, CERN, Geneva, May, 2011.

[74] S. Frixione, P. Nason, and B. R. Webber, *Matching NLO QCD and parton showers in heavy flavour production*, JHEP **08** (2003) 007, arXiv:hep-ph/0305252.

[75] G. Corcella et al., HERWIG *6.5 Release Note*, arXiv:[hep-ph/0210213].